Pergamon

Int. J. Heat Mass Transfer. Vol. 39, No. 12, pp. 2385–2400, 1996

0017–9310/96 $15.00+0.00

0017–9310(95)00347–9

Heat transfer in separated and impinging turbulent flows

K. HEYERICHS and A. POLLARD†
Department of Mechanical Engineering, Queen's University at Kingston, Ontario,
Canada K7L 3N6

(*Received* 13 *March* 1995 *and in final form* 15 *September* 1995)

Abstract—This paper considers both separating and impinging turbulent flows with heat transfer. The performance of the k–ε and k–ω turbulence models is assessed, especially how the low Reynolds number regions are resolved. In the case of the k–ε model, three wall functions and six low Reynolds number near-wall closures are evaluated. The turbulence models are solved in conjunction with the Reynolds-averaged momentum and energy equations using a control volume method and QUICK differencing scheme. The results indicate that the k–ω model demonstrates superior performance for prediction of convection heat transfer in complex turbulent flows and numerically is easy to implement. Copyright © 1996 Elsevier Science Ltd.

1. INTRODUCTION

The ability to predict turbulent flow and associated heat transfer by mathematical modelling is of considerable practical value. In general terms, the criteria for a good turbulence model are: minimum complexity (i.e. contain a minimum number of differential equations, empirical constants and functions but still provide sufficiently accurate and physically realistic results); robustness (i.e. promote stable convergence and not have difficulty resolving the steep gradients in near-wall regions); possess extensive universality (i.e. can be applied to a wide variety of flows without adjusting the empirical constants). For practical engineering calculations, two-equation turbulence models have become the most popular, since they are relatively simple to program and place much lower requirements on computer resources than other more complex models (e.g. algebraic and Reynolds stress models). Consequently, when cost effective, timely solutions of flows spanning large domains with complicated geometries are required, only two-equation models are currently practical.

The main difference between two-equation models is the treatment of near-wall regions and choice of the length scale variable, an equation for the transport of turbulence kinetic energy being common to all. As well, a significant problem with the selection of a turbulence model is that it is often difficult to assess those models available since they have been tested on different test cases using a variety of grid sizes and numerical schemes. It is therefore not clear which of the many proposed models provides the best performance, especially in the case of complex flows that involve impingement or boundary separation and reattachment. This paper attempts to resolve this issue by applying and comparing ten different models to three test cases, which all use a common numerical scheme.

2. THE MOMENTUM AND ENERGY EQUATIONS

The Reynolds stresses are related to the mean strain rate via an isotropic scalar turbulent viscosity, ν_t

$$\overline{u_i'u_j'} = \frac{2}{3}\delta_{ij}k - \nu_t\left(\frac{\partial u_i}{\partial x_j} + \frac{\partial u_j}{\partial x_i}\right). \tag{1}$$

The turbulent heat flux can be obtained using a gradient diffusion model

$$\overline{u_i h'} = -\frac{\nu_t}{\sigma_t}\frac{\partial h}{\partial x_i} \tag{2}$$

where σ_t is the turbulent Prandtl number.

The steady-state Reynolds averaged momentum and energy equations are then:

$$\frac{\partial(\rho u_i u_j)}{\partial x_i} = -\frac{\partial p}{\partial x_i} + \frac{\partial}{\partial x_j}\left[(\mu+\mu_t)\left(\frac{\partial u_i}{\partial x_j} + \frac{\partial u_j}{\partial x_i}\right)\right] \tag{3}$$

$$\frac{\partial(\rho u_i h)}{\partial x_i} = \frac{\partial}{\partial x_i}\left[\left(\frac{\mu}{\sigma} + \frac{\mu_t}{\sigma_t}\right)\frac{\partial h}{\partial x_i}\right]. \tag{4}$$

The turbulent viscosity ν_t is provided by the turbulence model. Two groups of two-equation models are considered in this paper: k–ε and k–ω turbulence models, a brief description of them is provided below for completeness.

---

† Author to whom correspondence should be addressed.

NOMENCLATURE

A_μ, A_ε	empirical constants
c_1	length scale constant
C_f	skin friction, table
C_p	specific heat at constant pressure [J kg^{-1} K^{-1}]
C_μ, C_1, C_2	k–ε turbulence model constants
D	diameter [m]
$\tilde{D}$	k–ε turbulence model additional term [m^2 s^{-3}]
D_h	hydraulic diameter [m]
E	additive contant in the velocity log-law, $E = 9.0$
$\hat{E}$	additive constant in the temperature log-law
$\tilde{E}$	k–ε turbulence model additional term [kg m^{-1} s^{-4}]
f	friction factor
f_μ, f_1, f_2	k–ε turbulence model damping functions, Table 2
G	generation rate of turbulent kinetic energy [m^2 s^{-3}]
h	time averaged enthalpy [J kg^{-1}]
$\hbar$	heat transfer coefficient [W m^{-2} K^{-1}]
h_w	time averaged wall enthalpy [J kg^{-1}]
H	general height parameter [m]
i	turbulence intensity, $i = \sqrt{(\overline{u_i'u_i'})}/u$
k	turbulent kinetic energy [m^2 s^{-2}]
$\tilde{k}$	thermal conductivity [W m^{-1} K^{-1}]
k^+	dimensionless turbulent kinetic energy, $k^+ = k/u_\tau^2$
l	length scale of turbulence [m]
l_μ	length scale of turbulence [m]
l_ε	length scale of turbulence [m]
L	general length parameter [m]
$\dot{m}_{in}$	mass flow rate [kg s^{-1}]
Nu	Nusselt number, $Nu = \hbar L/k$
p	time averaged pressure [Pa]
$\mathcal{P}$	Jayatilleke "Pee"-function
q	heat flux [W m^{-2}]
q_w	wall heat flux [W m^{-2}]
r	statistical correlation coefficient
R_β	k–ω turbulence model constant, $R_\beta = 8$
R_k	k–ω turbulence model constant, $R_k = 6$
R_t	turbulent Reynolds number
R_t^*	turbulent Reynolds number
R_w	k–ω turbulence model constant, $R_w = 2.7$
R_y	turbulent Reynolds number
Re	Reynolds number, $Re = \rho u L/\mu$
S_ε	Yap correction term
S_h	volumetric rate of convection heat transfer [W m^{-3}]
S_P	coefficient of ϕ_P in the linearized source term
St	Stanton number, $St = \hbar/\rho C_p u$
T	temperature [K]
T_w	wall temperature [K]
T_f	fluid temperature [K]

T^+	dimensionless temperature, $T^+ = \rho C_p(T_w - T)u_\tau/q_w$
u	time averaged x-direction velocity [m s^{-1}]
u_τ	wall friction velocity [m s^{-1}]
u'	fluctuating x-direction velocity [m s^{-1}]
u^+	dimensionless velocity
W	general width parameter [m]
W_1, W_2	variables used to express the expansion ratio of a channel [m]
x, y, z	coordinates
y^+	dimensionless distance.

Greek symbols

α_0, α_0^*	k–ω turbulence model constants, $\alpha_0 = 1/10$, $\alpha_0^* = \beta/3$
α, α^*	k–ω turbulence model closure coefficients
α_{eff}	effective thermal diffusivity [m^2 s^{-1}]
β	k–ω turbulence model constant, $\beta = 3/40$
β^*	k–ω turbulence model closure coefficient
β_1	grid uniformity determining parameter
ε	dissipation rate of turbulent kinetic energy [m^2 s^{-3}]
ε^+	dimensionless dissipation rate of turbulent kinetic energy, $\varepsilon^+ = \nu\varepsilon/u_\tau^4$
$\tilde{\varepsilon}$	dissipation variable [m^2 s^{-3}]
κ	von Karman's constant, $\kappa = 0.41$
$\hat{\kappa}$	constant appearing in temperature log-law
μ	molecular dynamic viscosity [kg m^{-1} s^{-1}]
μ_t	turbulent dynamic viscosity [kg m^{-1} s^{-1}]
ν	molecular kinematic viscosity [m^2 s^{-1}]
ν_t	turbulent kinematic viscosity [m^2 s^{-1}]
ρ	density [kg m^{-3}]
σ	molecular Prandtl number, $\sigma = C_p\mu/k$
σ_k, σ_ε	k–ε turbulence model constants
σ_k^*, σ_ω	k–ω turbulence model constants, $\sigma_k^* = 1/2$, $\sigma_\omega = 1/2$
σ_t	turbulent Prandtl number, $\sigma_t = 0.9$
τ	shear stress [N m^{-2}]
τ_w	wall shear stress [N m^{-2}]
ω	specific dissipation rate [s^{-1}].

Subscripts

i, j, k	indices for tensor notation
bulk	bulk flow conditions
J	jet inlet conditions
I	inlet conditions
m	mean flow conditions
P	central grid point under consideration
v	edge of the viscous sublayer
∞	free stream conditions.

Superscripts

	averaged quantity.

3. THE k–ε GROUP OF MODELS

The k–ε model relates the turbulence viscosity ν_t to the turbulence kinetic energy, k, and the turbulence dissipation rate, ε, using

$$\nu_t = C_\mu \frac{k^2}{\varepsilon} \tag{5}$$

where k and ε are defined as usual, equations for which are (see, for example, Patel *et al.* [1]):

$$\frac{\partial(\rho u_i k)}{\partial x_i} = \frac{\partial}{\partial x_i}\left[\left(\mu + \frac{\mu_t}{\sigma_k}\right)\frac{\partial k}{\partial x_i}\right] + \rho G - \rho\varepsilon \tag{6}$$

$$\frac{\partial(\rho u_i \tilde{\varepsilon})}{\partial x_i} = \frac{\partial}{\partial x_i}\left[\left(\mu + \frac{\mu_t}{\sigma_\varepsilon}\right)\frac{\partial \tilde{\varepsilon}}{\partial x_i}\right] + f_1 \rho C_1 \frac{\tilde{\varepsilon}}{k} G - f_2 C_2 \rho \frac{\tilde{\varepsilon}^2}{k} + \tilde{E} \tag{7}$$

where

$$G \equiv -\overline{u_i' u_j'} \frac{\partial u_i}{\partial x_j} \tag{8}$$

$$\varepsilon = \tilde{\varepsilon} + \tilde{D} \tag{9}$$

$$R_t = \frac{k^2}{\nu \tilde{\varepsilon}} \tag{10}$$

$$R_y = \frac{\sqrt{(k)}y}{\nu}. \tag{11}$$

The k–ε turbulence model is valid only in high Reynolds number regions. It is not applicable in regions close to solid walls where viscous effects predominate over turbulent ones. Two methods are commonly used to handle near-wall regions: wall functions or low Reynolds number modelling.

3.1. *Wall functions*

The wall function method, Launder and Spalding [2], assumes that close to a solid wall (but far enough from it that the effects of molecular transport can be considered negligible) the velocity and temperature profiles can be described by universal logarithmic velocity and temperature profiles. It is also assumed that in this region the turbulence is in a state of local equilibrium.

In all suggested variations of the wall function method, the turbulence kinetic energy in the near-wall cell is computed from the equation for k. The main difference between the various wall functions is the method used to calculate the generation and dissipation terms in the near-wall cell over which the governing equations are integrated. The simplest method is to assume that the turbulence variables (e.g. k, ε and the shear stress τ) are constant throughout the near-wall cell. Wall functions that use this approach are termed one-layer wall functions, which will be referred to here as WF1. In an attempt to improve the results obtained from the wall function technique, Chieng and Launder [3] proposed that the near-wall cell should be divided into two layers (i.e. the near-wall region is assumed to be composed of a viscous sublayer where turbulent stresses are negligible and a fully turbulent region where viscous transport can be ignored). This led to the development of the two-layer wall function (referred to by WF2).

When using the wall function technique, ε must also be solved or specified in the near-wall region. In the case of WF1 and WF2, ε in the near-wall cell is fixed at its equilibrium value. Amano [4] suggested that the generation and destruction terms in the ε equation should be evaluated in terms of the k equation rather than approximated under local equilibrium conditions; this model assumption is referred to as WF3.

Another approach that can be used to model the near-wall region is that employed by Chen and Patel [5]. This method combines the high Reynolds number k–ε model with the one equation model of Wolfshtein [6]. When using this Wolfshtein, Chen, Patel model (WCP) the calculation domain is broken into two regions. Region 1 includes the sublayer, the buffer layer and a part of the fully turbulent layer. The one-equation model of Wolfshtein is used in this region to account for the effects of viscosity near the wall. Region 2 is the fully turbulent region where the high Reynolds number k–ε model can be applied in the usual fashion. The separation point between the two regions is chosen along the grid line where the turbulence Reynolds number R_y is approximately equal to 250, see Chen and Patel [5].

3.2. *Low Reynolds number modelling*

To improve further the modelling of the near-wall regions several extensions to the high Reynolds number k–ε model have been suggested. Patel *et al.* [1] review eight different low Reynolds number models and conclude that the models of Launder and Sharma [7], Lam and Bremhorst [8] and Chien [9] performed considerably better than others. Yap [10] further refined the Launder and Sharma model by including an additional length scale correction term into a modified form of the ε equation, the $\tilde{\varepsilon}$ equation. Myong and Kasagi [11] introduced a low Reynolds number model that demonstrated improved ability to predict heat transfer in pipe flows. These models have been selected for further evaluation in this study.

The low Reynolds number k–ε model incorporates functions f_μ, f_1, f_2 and, in some cases, extra terms $\tilde{D}$ and $\tilde{E}$. Different formulae have been suggested to calculate the above terms and a summary of the boundary conditions, constants, damping functions and additional terms used in the models selected for evaluation in this study are listed in Tables 1–5. The equations used to calculate the wall shear stress and heat flux are given in Table 6.

4. THE k–ω MODEL

The k–ω turbulence model is similar to the low Reynolds number k–ε model with ε replaced by ω,

Table 1. Boundary conditions and constants used in the k–ε turbulence model

Model	Designation	k_w-B.C.	ε_w-B.C.	C_μ	C_1	C_2	σ_k	σ_ε
High Reynolds number	HRN			0.09	1.44	1.92	1.0	1.3
Chien	CH	0	0	0.09	1.35	1.80	1.0	1.3
Lam and Bremhost	LB	0	$\partial\varepsilon/\partial y = 0$	0.09	1.44	1.92	1.0	1.3
Launder and Sharma	LS	0	0	0.09	1.44	1.92	1.0	1.3
Launder *et al.*	LSY	0	0	0.09	1.44	1.92	1.0	1.3
Myong and Kasagi	MK	0	$\partial\varepsilon/\partial y = 0$	0.09	1.40	1.80	1.4	1.3

Table 2. Damping functions used in the k–ε turbulence model

Model	f_μ	f_1	f_2
HRN	1.0	1.0	1.0
CH	$1-\exp(-0.0115y^+)$	1.0	$1-0.22\exp\left[-\left(\frac{R_t}{6}\right)^2\right]$
LB	$[1-\exp(-0.0165R_y)]^2 \times\left(1+\frac{20.5}{R_t}\right)$	$1+\left(\frac{0.05}{f_\mu}\right)^3$	$1-\exp(-R_t^2)$
LS	$\exp\left(\frac{-3.4}{(1+R_t/50)^2}\right)$	1.0	$1-0.3\exp(-R_t^2)$
LSY	$\exp\left(\frac{-3.4}{(1+R_t/50)^2}\right)$	1.0	$1-0.3\exp(-R_t^2)$
MK	$\left[1+\frac{3.45}{\sqrt{R_t}}\right] \times\left[1-\exp\left(\frac{-y^+}{70}\right)\right]$	1.0	$\left[1-\frac{2}{9}\exp\left\{-\left(\frac{R_t}{6}\right)^2\right\}\right] \times\left[1-\exp\left(\frac{-y^+}{5}\right)\right]^2$

Table 3. Additional terms used in the k–ε turbulence model

Model	$\tilde{D}$	$\tilde{E}$
HRN	0	0
CH	$2\mu\frac{k}{y^2}$	$2\mu\left(\frac{\bar{\varepsilon}}{y^2}\right)\exp(-0.5y^+)$
LB	0	0
LS	$2\mu\left(\frac{\partial\sqrt{k}}{\partial y}\right)^2$	$2\frac{\mu\mu_t}{\rho}\left(\frac{\partial^2 u}{\partial y^2}\right)^2$
LSY	$2\mu\left(\frac{\partial\sqrt{k}}{\partial y}\right)^2$	$2\frac{\mu\mu_t}{\rho}\left(\frac{\partial^2 u}{\partial y^2}\right)^2+0.83\rho\left(\frac{\tilde{\varepsilon}^2}{k}\right)\left(\frac{k^{3/2}}{c_l y\tilde{\varepsilon}}-1\right)\left(\frac{k^{3/2}}{c_l y\tilde{\varepsilon}}\right)^2$
MK	0	0

which represents the frequency of the vorticity fluctuations. It is defined:

$$\omega = \frac{\varepsilon}{k\beta^*}. \tag{12}$$

Several different versions have been proposed, based on the work of Kolmogorov [12], extended by Spalding [13] and Saiy [14] and Saffman [15]; however, the k–ω version of Wilcox [16] has recently been demonstrated to be particularly promising and has therefore been

Table 4. Near-wall models used with the high Reynolds number k–ε turbulence model

Near-wall Model	Designation	Effective region	k_w-B.C.	ε_w-B.C.	Turbulent viscosity
One-layer wall function	WF1	Near-wall cell	$\frac{\partial k}{\partial y}=0$	—	$\nu_t = C_\mu \frac{k^2}{\varepsilon}$
Two-layer wall function	WF2	Near-wall cell	$\frac{\partial k}{\partial y}=0$	—	$\nu_t = C_\mu \frac{k^2}{\varepsilon}$
Two-layer wall function	WF3	Near-wall cell	$\frac{\partial k}{\partial y}=0$	$\frac{\partial \varepsilon}{\partial y}=0$	$\nu_t = C_\mu \frac{k^2}{\varepsilon}$
Wolfshtein, Chen and Patel	WCP	$R_y<250$	$k=0$	—	$\nu_t = C_\mu \sqrt{k} l_\mu$ $l_\mu = c_1 y\left[1-\exp\left(\frac{-R_y}{A_\mu}\right)\right]$ $A_\mu = 70$

Table 5. Calculation of k and ε using near-wall models

Model	k-equation G and ε terms	ε-Calculation
WF1	$G = \frac{\tau_w^{3/2}}{\rho^{1/2}\kappa y_P}$ $\varepsilon = \frac{k_P^{3/2}}{c_1 y_P}$	Fixed at equilibrium value $\varepsilon_P = \frac{k_P^{3/2}}{c_1 y_P}$
WF2	$G = \frac{\tau_\omega^{3/2}}{\rho^{3/2}\kappa y_n}\ln\left(\frac{y_n}{y_v}\right)+\frac{\tau_\omega}{\rho}\left(1-\frac{y_v}{y_n}\right)\frac{\partial v}{\partial y}$ $\varepsilon = \frac{2\nu k_v}{y_n y_v}+\frac{k_P^{3/2}}{c_1 y_n}\ln\left(\frac{y_n}{y_v}\right)$	Fixed at equilibrium value $\varepsilon_P = \frac{k_P^{3/2}}{c_1 y_P}$
WF3	$G = \frac{\tau_w^{3/2}}{\rho^{3/2}\kappa y_n}\ln\left(\frac{y_n}{y_v}\right)+\frac{\tau_\omega}{\rho}\left(1-\frac{y_v}{y_n}\right)\frac{\partial v}{\partial y}$ $\varepsilon = \frac{2\nu k_v}{y_n y_v}+\frac{k_P^{3/2}}{c_1 y_n}\ln\left(\frac{y_n}{y_v}\right)$	ε-equation with $C_1 \frac{\varepsilon}{k} G = \frac{c_1 \tau_w k_P^{1/2}}{\rho c_1 y_n}\left[\frac{\tau_\omega^{1/2}}{\rho^{1/2}\kappa}\left(\frac{1}{y_v}-\frac{1}{y_n}\right)+\ln\left(\frac{y_n}{y_v}\right)\frac{\partial v}{\partial y}\right]$ $C_2 \frac{\varepsilon^2}{k} = C_2\left[\frac{12\nu^2 k_v}{y_n y_v^3}+\left(\frac{k_P^2}{c_1^2 y_v y_n}\right)(1-y_v/y_n)\right]$
WCP	No modification	$\varepsilon = \left(\frac{k^{3/2}}{l_\varepsilon}\right)$ $l_\varepsilon = c_1 y\left[1-\exp\left(\frac{-R_y}{A_\varepsilon}\right)\right]$ $A_\varepsilon = 2c_1$

selected for use in the present study. The equations that constitute the k–ω model (WX) are Wilcox [16]:

$$\frac{\partial(\rho u_i k)}{\partial x_i} = \frac{\partial}{\partial x_i}\left[(\mu+\sigma_k^*\mu_t)\frac{\partial k}{\partial x_i}\right]+\rho G-\beta^*\rho\omega k \tag{13}$$

$$\frac{\partial(\rho u_i \omega)}{\partial x_i} = \frac{\partial}{\partial x_i}\left[(\mu+\sigma_\omega\mu_t)\frac{\partial \omega}{\partial x_i}\right]+\rho\alpha\frac{\omega}{k}G-\beta\omega^2 \tag{14}$$

where

$$\mu_t = \alpha^*\rho\frac{k}{\omega} \tag{15}$$

$$G \equiv -\overline{u_i' u_j'}\frac{\partial u_i}{\partial x_j} \tag{16}$$

$$R_t^* = \frac{\rho k}{(\omega\mu)}. \tag{17}$$

The k and ω equations are essentially a direct trans-

Table 6. Calculation of wall shear stress and heat flux

Variable	Wall functions	Low Reynolds number models
Shear stress	$\tau_w = \dfrac{u_P \kappa \rho C_\mu^{1/4} k_P^{1/2}}{\ln\left(\dfrac{E \rho y_P C_\mu^{1/4} k_P^{1/2}}{\mu}\right)}$	$\tau_w = \mu \dfrac{\partial u}{\partial y}$
Heat flux	$\dfrac{q_w}{\rho u_P (h_P - h_w)} = \dfrac{\tau_w/(\rho u_P^2)}{\sigma_t\{1 + \mathscr{P}\sqrt{[\tau_w/(\rho u_P^2)]}\}}$ $\mathscr{P} = 9.24[(\sigma/\sigma_t)^{0.75} - 1][1 + 0.28\exp(-0.007\sigma/\sigma_t)]$	$q_w = \dfrac{\mu}{\sigma} \dfrac{\partial h}{\partial y}$

Table 7. Constants and damping functions used in Wilcox k–ω model

Designation:	WX	α_0	1/10
k_w–B.C.	0	ω_w B.C.	$6\nu/\beta y^2$
σ_k^*	1/2	σ_ω	1/2
β	3/40	α_0^*	$\beta/3$
R_β	8	R_k	6
R_w	2.7	α	$\dfrac{5}{9}\dfrac{\alpha_0 + R_t^*/R_w}{1 + R_t^*/R_w}(\alpha^*)^{-1}$
α^*	$\dfrac{\alpha_0^* + R_t^*/R_k}{1 + R_t^*/R_k}$	β^*	$\dfrac{9}{100}\dfrac{5/18 + (R_t^*/R_\beta)^4}{1 + (R_t^*/R_\beta)^4}$

form of the low Reynolds number k–ε model with the addition of transition specific closure coefficients α and β. The boundary conditions, constants and damping functions used in conjunction with the k–ω model are given in Table 7. The wall shear stress and heat flux are calculated in the same way as for the low Reynolds number k–ε models.

5. NUMERICAL METHODS

The equation set consisting of the momentum, mass, energy and turbulence model equations was discretized using the control volume method, details of which can be conveniently found in, for example, Patankar [17]. The convection terms in the momentum equations were approximated using a form of the three-point QUICK scheme that closely follows the work of Pollard and Siu [18] (i.e. QUICKER). The convection terms for the scalar variables were computed using Hybrid Differencing of Spalding [19]. The SIMPLE algorithm in the form given by Van Doormaal and Raithby [20], with a standard TDMA solver, were used.

6. PRESENTATION AND DISCUSSION OF RESULTS

To assess and provide a benchmark, the models are first applied to plane channel flow, $Re_{D_h} = 100\,000$. The velocity log-law and correlations for skin friction and heat transfer are used to bench-mark the turbulence model performance. The models are then applied to two complex turbulent flows: a single turbulent impinging jet $Re_W = 10\,000$, $H/W = 2.6$ and backward facing step flow $Re_H = 28\,000$. These geometrically simple test cases contain stagnation and recirculation zones, which provide stringent conditions for testing turbulence models. Convection heat transfer along solid walls is determined by the variation of effective diffusivity within the immediate vicinity of the wall, accurate prediction of the latter is crucial for accurate prediction of the former. For the case of the turbulent impinging jet the calculated results are compared to Nusselt number data of Cadek [21], Das [22], Gardon and Akfirat [23] and van Heiningen [24]. For the backward facing step case the model predictions are compared to the Stanton number and skin friction data measured by Vogel and Eaton [25].

Table 8. Grid size (axial × wall normal) used for test cases

Test case	Wall functions	Low Reynolds number models
Channel flow	242 × 20	242 × 60
Impinging jet	92 × 30	92 × 100
Backward facing step	175 × 50	175 × 70

The grid sizes (non-uniformly distributed) used for the test cases are provided in Table 8. These were determined after extensive grid refinement tests revealed little dependence on additional refinement.

6.1. *Channel flow*

Table 9 presents the skin friction C_f and the Nusselt number Nu results for channel flow $Re_{D_h} = 100\,000$. The data are presented from $L/D_h = 60$ where it can be assumed that the flow is fully developed and independent of initial conditions. The walls are at constant temperature. The percentage errors $\%C_f$ and $\%Nu$ are calculated relative to the values obtained from the friction factor correlation, Özişik [26]:

$$\frac{1}{\sqrt{f}} = 2.0\log(Re_{D_h}\sqrt{f}) - 0.8 \qquad (18)$$

and Dittus–Boelter correlation

Table 9. Skin friction and Nusselt number results for the channel flow test case

Model	C_f	% C_f	Nu	% Nu
Correlation	0.00450	—	200.6	—
WF1	0.00453	0.7	163.1	−18.7
WF2	0.00440	−2.1	159.4	−20.5
WF3	0.00454	0.9	162.4	−19.0
CH	0.00445	−1.0	187.9	−6.3
LB	0.00480	6.8	208.9	4.2
LS	0.00440	−2.2	187.7	−6.4
LSY	0.00483	7.4	207.7	3.6
MK	0.00471	4.7	205.0	2.2
WCP	0.00465	3.3	198.2	−1.2
WX	0.00469	4.3	203.7	1.6

$$Nu = 0.023\, Re_{D_h}^{0.8} \sigma^{0.4} \qquad (19)$$

where σ is the Prandtl number. All models, with the exception of LB and LSY, predict C_f ($f = C_f/2$) within 5% of that given by equation (18). The Nusselt number is predicted to within 5% of (19) by all models, except those of CH, LS and the wall functions (WF1, WF2 and WF3).

Figure 2 shows the normalised velocity u^+ and temperature T^+ profiles predicted by the wall functions, where the correlations of Kader [27] are used for comparison. The wall functions accurately reproduce the log-law and predict C_f within $\approx 2\%$, as expected. The differences resulting from each wall function formulation are minor, but it can be observed that the two-layer model leads to a lower C_f value relative to the one-layer model. This occurs since the one-layer approach assumes that turbulence is produced throughout the near-wall control volume, whereas the two-layer approach calculates the production of turbulence beyond the viscous sublayer. The two-layer

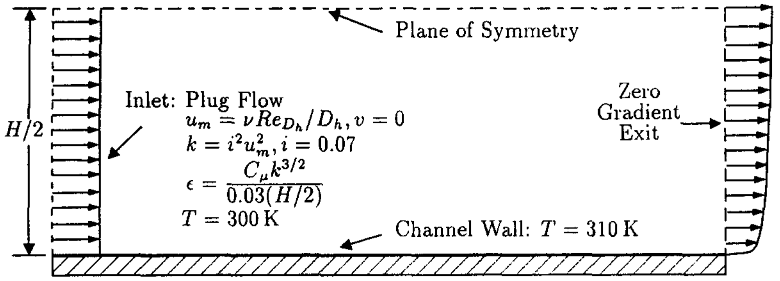

The channel flow test case

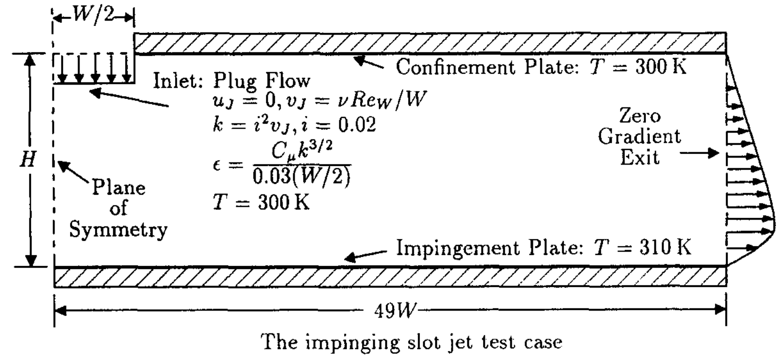

The impinging slot jet test case

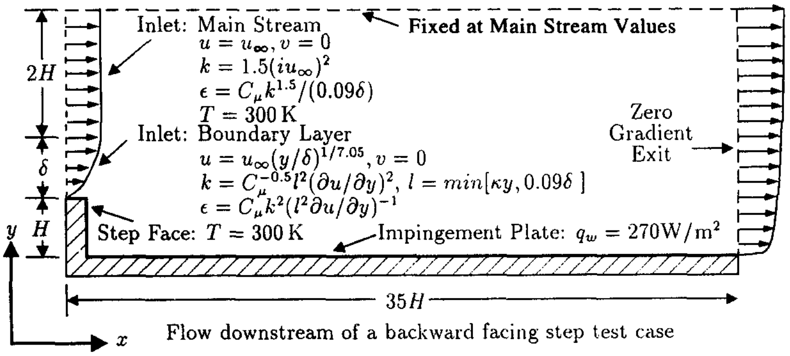

Flow downstream of a backward facing step test case

Fig. 1. Test case boundary conditions.

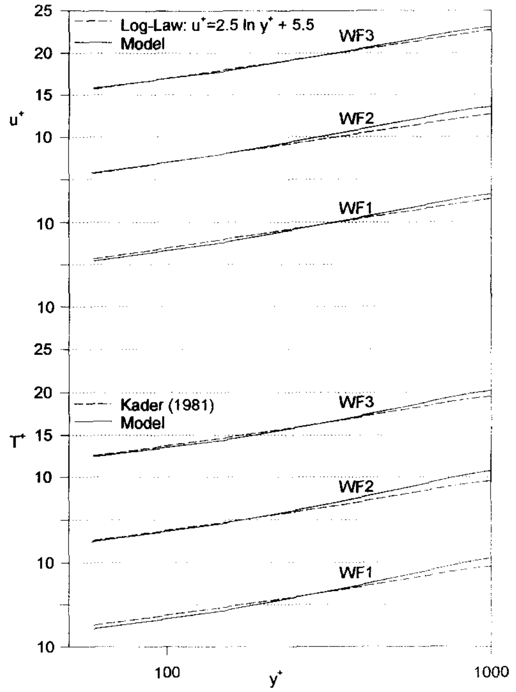

Fig. 2. u^+ and T^+ profiles calculated using wall functions.

model predicts slightly lower turbulence levels and therefore lower C_f values. Calculation of ε in the near-wall control volume using the method suggested by Amano [4], as opposed to approximating it at its equilibrium value, results in a lower value of ε.

The wall heat flux, calculated using wall functions, Launder and Spalding [2], employs the temperature log-law relationship of Jayatilleke [28], which shows good agreement to the T^+ data of Kader [27]. This method, however, calculates $Nu \approx 19\%$ low relative to the Dittus–Boelter correlation and the minor differences between WF1, WF2 and WF3 are a direct consequence of the C_f predictions.

Figure 3 demonstrates that LRN models strongly link skin friction to heat transfer. For example, models CH and LS underpredict C_f and therefore underestimate Nu. Conversely, LB and LSY substantially overestimate C_f and have the highest overestimate of Nu. This is expected since it has long been established that for boundary layer flows Nu is correlated to C_f through, for example, the Reynolds analogy. C_f is calculated, using LRN models, from the slope of the velocity profile at the wall. Since C_f is strongly correlated to the log-law, Patel *et al.* [1], it follows that Nu should also correlate with the log-law. Figure 4(a) indicates that WCP provides the best fit to the log-law and consequently also predicts Nu most accurately. The models LB, LSY and MK substantially underestimate the log-law and display the highest overestimate of Nu. Figure 4(b) compares the predictions of T^+ using LRN models. All these models calculate T^+ below the data of Kader [27] and therefore predict significantly higher Nu values relative to the wall functions. Since the rate of convection heat transfer is determined to a very large extent by the variation of effective thermal diffusivity (i.e. $\chi_{\text{eff}} = \nu/\sigma + \nu_t/\sigma_t$) within the immediate vicinity of the wall [29], it can be expected that Nu and the temperature profile T^+ are strongly influenced by the ability of the turbulence model to predict ν_t in the near-wall region and the value selected for σ_t. Figure 4(c) shows the predicted near-wall turbulent viscosity normalized by the laminar viscosity relative to data summarised in Patel *et al.* [1]. The models WX and WCP show strong agreement between ν_t data and Nu. Conversely, the models LB and LSY that substantially over-predict ν_t also overestimate Nu.

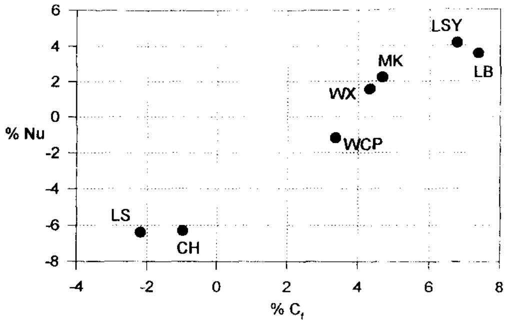

Fig. 3. Correlation between C_f and Nu for various low-Reynolds number models.

Figure 5(a) shows the effect of σ_t on the temperature distribution calculated using the WCP model. Increasing σ_t pushes the T^+ profile closer to those data of Kader. This in turn results in an almost linear decrease in Nu as shown in Fig. 5(b). The profile of σ_t in the near-wall region has been a matter of conjecture; for example, direct numerical simulation of Kasagi *et al.* [30] indicates that $\sigma_t = 1.02$ at the wall, increases to 1.1 at $y^+ \approx 50$ and then gradually decreases with distance from the wall, which is noticeably different from the constant value, $\sigma_t = 0.9$, usually used. A correlation in which σ_t (R_t) would be useful; however, experiments that accurately determine the distribution of T^+, σ_t and Nu at the wall would be needed.

Figures 6(a) and (b) compare the predicted near-wall k^+ and ε^+ profiles to data compiled by Patel *et al.* [1]. Models WX and LB reproduce best the distribution of k^+ while MK and WCP show the best agreement to ε^+. No model predicts well both variables, indicating that further optimization of the near-wall damping functions is still required. In particular, these figures indicate relatively poor performance by CH, LS and LSY. This can be related to the $\tilde{D}$ and $\tilde{E}$ terms that represent near-wall effects. Consequently CH, LS and LSY poorly predict Nu. Figure 6(b) also shows that WX displays a rather peculiar ε^+ profile in the buffer layer. This effect results from the β^* term used to convert from ε to ω.

Myong and Kasagi [11] and Yeung and Pollard [31] suggest the constants used in the standard k–ε model of Launder and Spalding [2], $C_1 = 1.44$, $C_2 = 1.92$, $\sigma_k = 1.0$, $\sigma_\varepsilon = 1.3$ overestimate ν_t in the central region

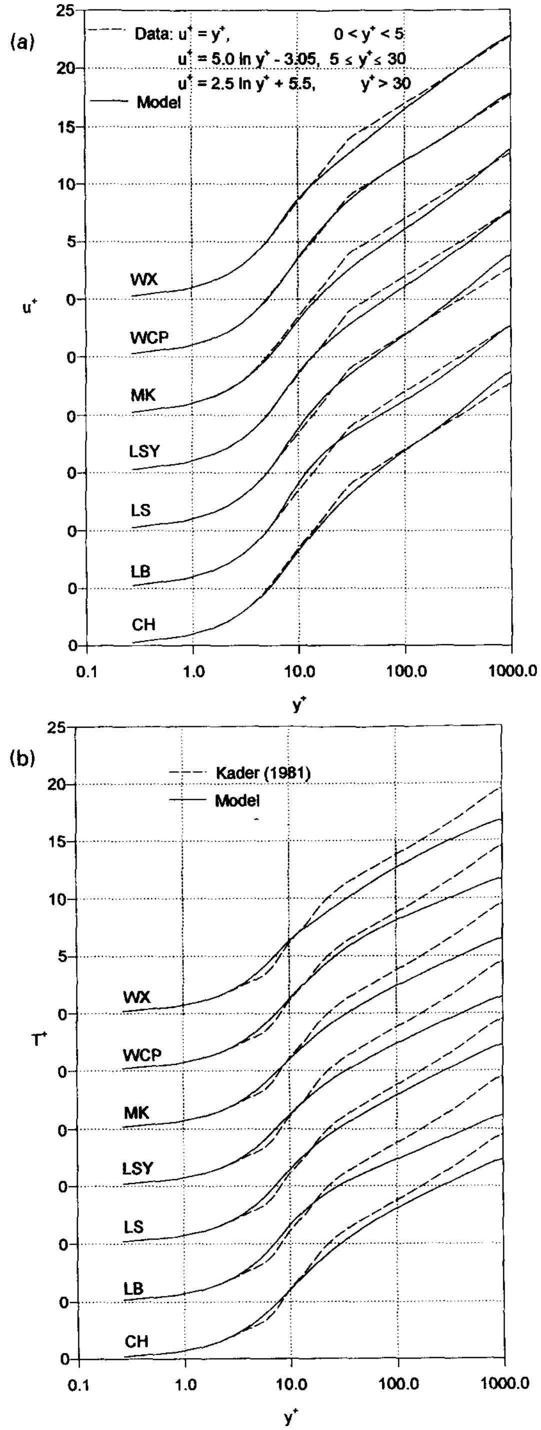

Fig. 4. Channel flow—(a) u^+ vs y^+ ; (b) T^+ vs y^+ ; (c) ν_t/ν vs y^+.

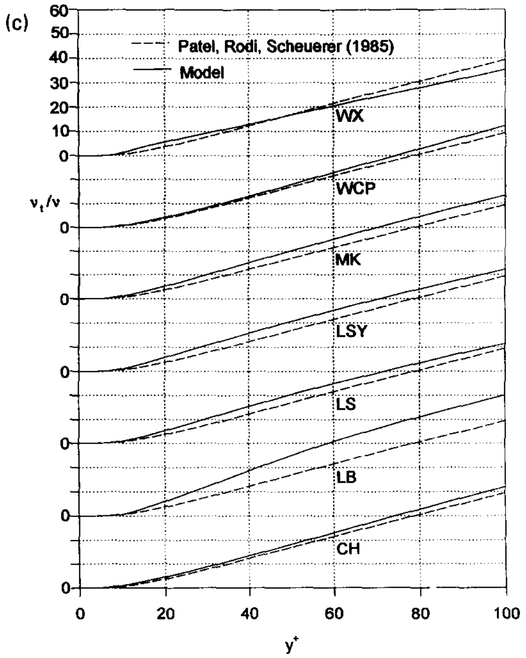

Fig. 4—*continued.*

of a pipe or channel. Figure 7 shows the effect of the model constants on the ratio ν_t/ν for a channel flow $Re_{D_h} = 81\,270$. Data of ν_t/ν, Hussain and Reynolds [32], reaches a maximum value of ≈ 80 at $y/H = 0.45$ and then decreases to ≈ 64 at the centreline. The WCP model, which uses the standard constants predicts ν_t/ν increasing to ≈ 87 and therefore overestimates the data by 35% at the centreline. The curve predicted by WCP is also representative of the results obtained from the models of CH, LB, LS and LSY. Changing the WCP model constants to those suggested by Yeung and Pollard [31], $C_1 = 1.48$, $C_2 = 1.92$, $\sigma_k = 1.25$, $\sigma_\varepsilon = 1.2$ results in ν_t/ν curve that closely follows the data and decreases the predicted value of ν_t/ν at the centreline by 27%. The MK model produces a similar effect for which ν_t/ν is 22% lower than the WCP model at the centreline. It should also be noted

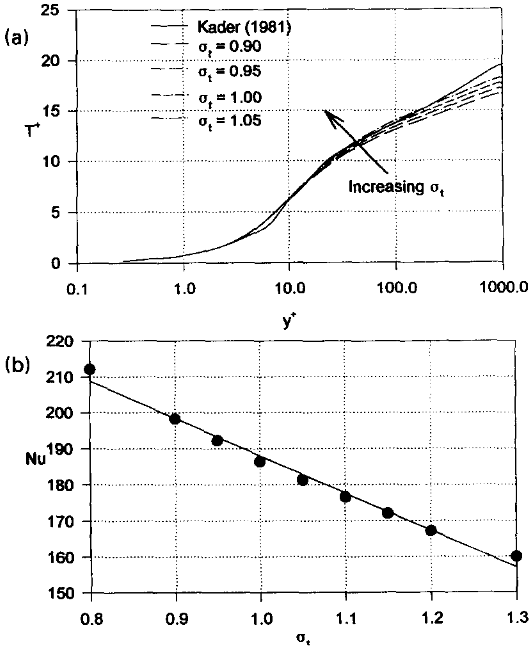

Fig. 5. Channel flow, WCP model (a) effect of σ_t on the T^+ ; (b) effect of σ_t on Nu.

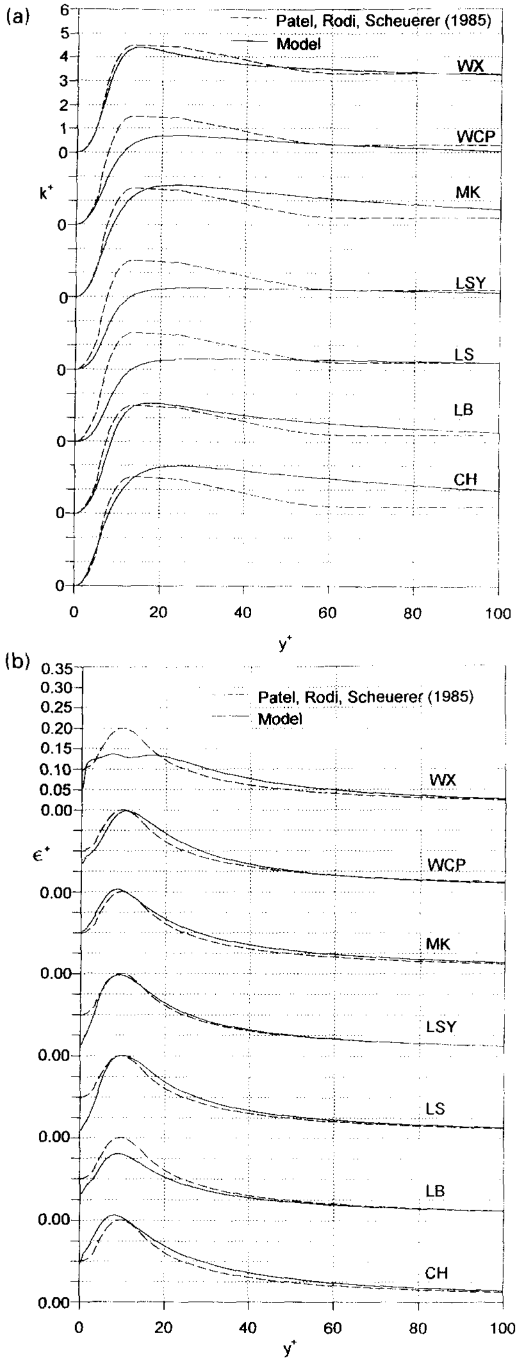

Fig. 6. Channel flow— (a) k^+ vs y^+; (b) ε^+ vs y^+.

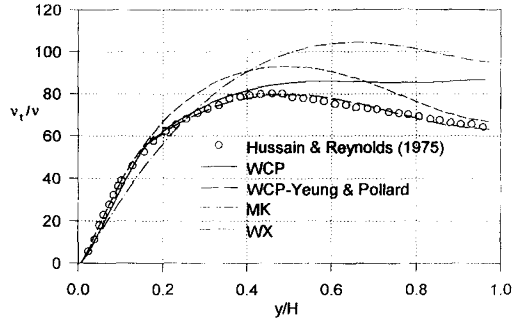

Fig. 7. Effect of model constants on ν_t/ν distribution.

that the choice of constants in WX leads to higher values of ν_t/ν for the entire central region of the channel and overestimates the data by 49% at the centreline. This would indicate that further optimisation of the WX model constants is required.

The foregoing indicate that all models predict reasonably well boundary layer flows. This could be anticipated since the models were developed for this type of flow. The models of WCP and WX calculate the turbulent convection heat transfer rate better than the other models tested, predicting Nu with less than 2% error. Review of the WCP and WX models predictions of the turbulence variables k^+, ε^+ and ν_t indicates that further refinement of the model constants and near-wall damping functions is required.

6.2. *Impinging slot jet flow*

The calculated impingement plate Nu profiles are compared to the experimental data of Gardon and Akfirat [23], Cadek [21], Das [22] and van Heiningen [24] for the impinging slot jet test case $Re = 10\,000$, $H/W = 2.6$, Fig. 8(a), and the corresponding impingement plate C_f profiles are shown in Fig. 8(b). Jet inlet conditions were uniform mean flow with 2% turbulence intensity, the constant impingement plate temperature being 10 K above both the inlet fluid and confinement plate temperature (both at 300 K). Along the impingement plate, there exists a stagnation region from which develops a wall jet. At the stagnation point $C_f = 0$ and Nu is a maximum ≈ 43 due to impingement of large-scale eddies that form during jet development. Around the stagnation point, the fluid is caused to alter its direction, undergoing strong acceleration, which results in a rapid increase in C_f distal to impingement. A boundary layer develops along the impingement plate and Nu displays a secondary peak ≈ 27 at $H/W \approx 7$. Decreases in the values of C_f and Nu result from flow deceleration with distances farther removed from impingement with a gradual diminution with $Nu \approx 15$ at $x/W = 20$. The impinging slot jet configuration is a test case that evaluates assumptions made in near-wall modelling.

To rank each models' ability to predict, on average, the Nu distribution, the correlation coefficient r is calculated, Table 10, where $r = 1$ the predicted values fit exactly the experimental data. Table 10 presents, as well, the percentage error in the predicted maximum Nu in the stagnation region, Nu at the secondary peak and Nu downstream at $x/W = 20$. Figure 8(a) and Table 10 indicate that the Nu profile predicted by the WX model has the strongest agreement ($r = 0.98$) to the data set. Indeed, WX is the only model that determines the wall-proximity effects based on turbulence variables via the turbulence Reynolds number R_t. All other models determine the near-wall turbulence using

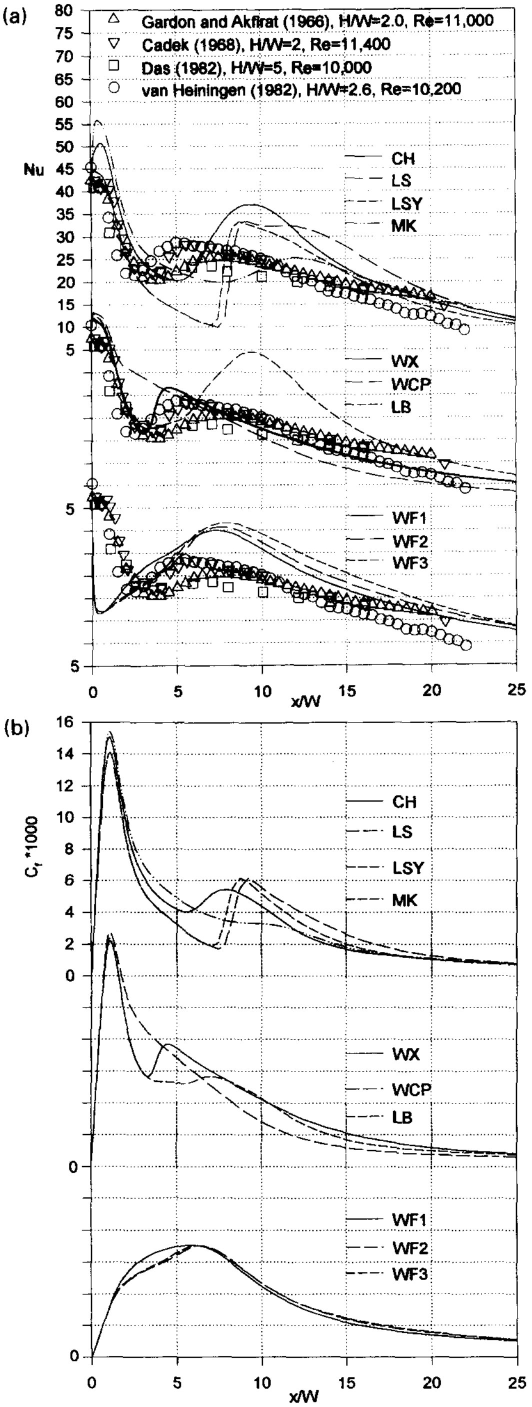

Fig. 8. Impinging jet: (a) impingement plate Nu vs x/W; (b) impingement plate C_f vs x/W.

functions that contain either u_τ, distance from the wall functions based on the turbulence variables extrapolate better to conditions far from equilibrium.

All low Reynolds number models correlate reasonably well to those data considered, having correlation coefficients greater than 0.77; however, the wall functions WF1, WF2 and WF3 have low negative r values, which indicate their predictions have little statistical correlation to the data. Therefore, wall functions are not recommended for this type of flow. In addition, the refined wall functions WF2 and WF3 do not improve the prediction of Nu or C_f relative to WF1. The wall functions all perform poorly in the stagnation region where the assumptions used in their derivation are certainly not valid.

The CH and MK models also perform poorly in the stagnation region: they overestimate the maximum Nu and predict its location to occur away from the stagnation point at $x/W \approx 0.5$. The Nu profiles appear to be influenced by the initial step rise and off-stagnation peak shown by the profiles in C_f. Similar to the wall functions, the CH and MK models calculate the wall-proximity effects based on y^+ and therefore assume that turbulence in this region can be related to u_τ. The poor performance of the CH and MK models demonstrate that low Reynolds number models with near-wall damping functions based on y^+ are not suitable for prediction of heat transfer in the vicinity of a stagnation point.

All models predict poorly both the magnitude and the location of the secondary peak in the distribution of Nu; note, too, that the profiles of Nu and C_f are similar. The WCP model fails completely to predict the secondary peak in Nu, which indicates that, to accurately predict this type of flow, a length scale determining transport equation is required, even in the near-wall region. The WX model has the strongest correlation to the data set: it predicts Nu in this region better than other models.

Far downstream (i.e. $x/W > 20$) the flow resembles developing channel flow and the predicted C_f and Nu profiles from all models converge to similar values. The Nu results can be correlated to C_f but the value of C_f predicted by each model does not follow the same order as that found in the channel flow test case. Thus it appears that the C_f and Nu predictions in this region are strongly affected by the capability of a model to capture the physical phenomena upstream of this region. The addition of the Yap correction term to the LS model slightly improves the prediction Nu beyond the secondary peak.

The impinging slot jet test case indicates that, from the models considered, only the WX model adequately predicts turbulent convection heat transfer in a flow that involves stagnation followed by acceleration and deceleration. Wall functions and low Reynolds number models, which calculate the near-wall turbulence based on u_τ or distance from the wall, perform poorly and are not recommended for this type of flow.

6.3. *Flow downstream of a backward facing step*

The flow over a backward facing step was computed using inlet and boundary conditions given by Vogel and Eaton [25]. Figures 9(a)–(d) compare the calculated impingement plate St profiles to the experimental data of Vogel and Eaton [25] for the backward facing step test case $Re_H = 28\,000$, $\delta/H = 1.1$. Figure 10 compares the impingement plate C_f profiles pre-

Table 10. Nusselt number results for the impinging jet test case

Model	Correlation coefficient r	% Nu at stagnation region	% Nu at secondary peak	% Nu @ $x/W = 20$
WF1	−0.38	−27.8	32.0	9.6
WF2	−0.35	−21.5	34.9	18.0
WF3	−0.41	−21.6	38.4	25.8
CH	0.92	18.8	39.9	6.1
LB	0.92	12.5	49.1	8.0
LS	0.77	5.0	26.1	18.6
LSY	0.84	4.9	25.3	−3.6
MK	0.92	30.6	−4.7	11.1
WCP	0.91	12.8	–	−30.5
WX	0.98	9.9	19.5	−13.0

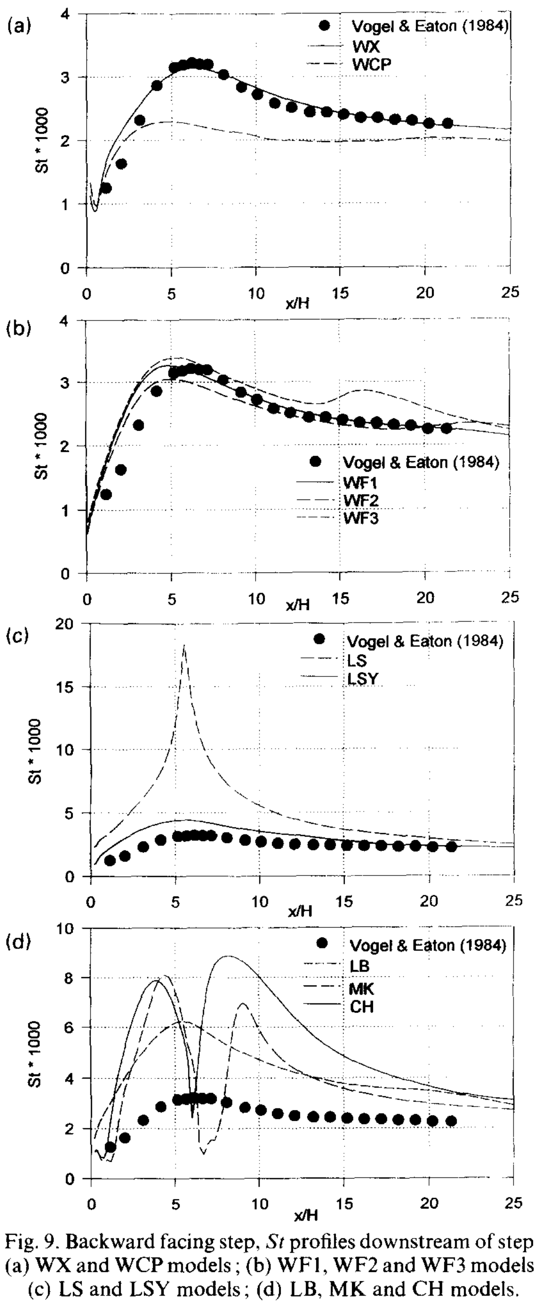

Fig. 9. Backward facing step, St profiles downstream of step: (a) WX and WCP models; (b) WF1, WF2 and WF3 models; (c) LS and LSY models; (d) LB, MK and CH models.

dicted by each model to the experimental data of Adams *et al.* [33] and Vogel and Eaton [25].

The experimental data reveal that the flow along the impingement plate can be divided into three zones: recirculation region, reattachment region and redeveloping near-wall flow. In the recirculation region, St has not reached its peak around flow attachment, C_f is negative. The peak $St \approx 0.0032$ occurs at $0.67H$ upstream (relative to the mean flow direction) of reattachment. The reattachment point is located $6.67H$ downstream of separation. At reattachment C_f passes through zero and then increases downstream. Vogel and Eaton [25] attribute the high heat transfer rate in the vicinity of reattachment to the impingement of energetic free shear layer eddies and diminution of the viscous sublayer where heat transfer is largely governed by molecular diffusion. Downstream of reattachment St decreases to levels typically found in a turbulent boundary layer, which is probably due to

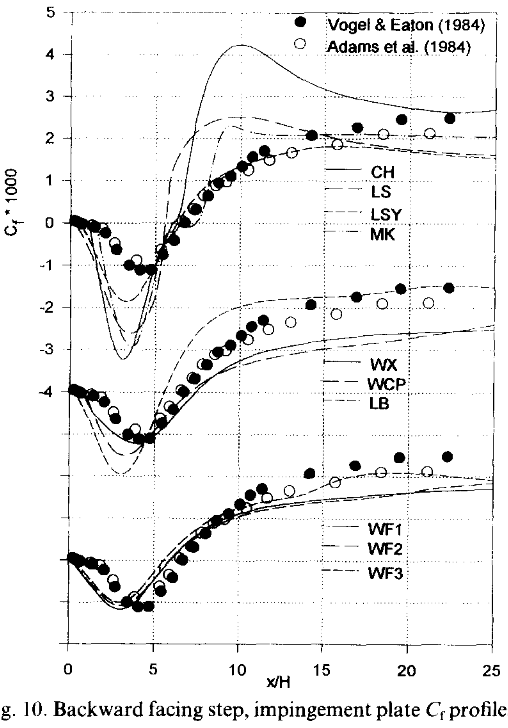

Fig. 10. Backward facing step, impingement plate C_f profiles.

Table 11. Stanton number results for the backward facing step case

Model	Correlation coefficient r	% St at maximum St	% x/H at maximum St	% St at $x/H = 20$
WF1	0.82	1.6	−17.8	0.6
WF2	0.85	−5.2	−17.8	0.6
WF3	0.87	5.3	−11.7	14.3
CH	0.54	175.6	34.7	61.7
LB	0.80	93.5	−7.6	53.9
LS	0.73	469.0	−7.6	30.7
LSY	0.77	37.6	−7.6	3.8
MK	0.36	151.8	−26.8	31.8
WCP	0.82	−28.7	−22.9	−10.5
WX	0.95	−2.5	4.0	−0.7

the thickening of the viscous sublayer. The backward facing step configuration evaluates how well the turbulence models predict a flow that involves reattachment of a separated turbulent boundary layer.

In order to quantify and rank each model's ability to reproduce the St and C_f data of Vogel and Eaton [25], the correlation coefficients are given in Tables 11 and 12. Table 11 also shows the percentage error in the predicted: maximum St, location of the maximum St and the value of St downstream of reattachment at $x/H = 20$, this location being arbitrarily chosen. Table 12 shows the percentage error in the predicted minimum C_f in the recirculation region, C_f downstream at $x/H = 20$ and the separated flow reattachment length.

Figure 9(a) and Table 11 clearly indicate that the WX model predicts the St profile significantly better than any of the other models tested. The WX model has the strongest correlation to the data ($r = 0.95$) and reproduces the maximum St, the location of the maximum St and the St downstream of the maximum peak with less than 5% error. The one-equation near-wall formulation of WCP shows reasonable correlation to the data ($r = 0.82$) but fails to predict the peak in the St profile, which occurs near reattachment. This result indicates that in the vicinity of reattachment the length scale in the near-wall region is not adequately described by Wolfshtein's model.

Figure 10 and Table 12 indicates that the C_f profile is best reproduced by the WX model, which displays the strongest correlation to the C_f data ($r = 0.99$); moreover, it predicts C_f in the recirculating flow region better than any of the other models. The reattachment length is calculated most accurately by the models of LSY and WCP. All models poorly predict C_f beyond reattachment where a boundary layer begins to develop along the impingement plate.

Figure 9(b) and Table 12 indicate that the wall functions WF1 and WF2 and WF3 predict the St profile well, showing a better correlation to the data than all low Reynolds number models, except WX. Johnson and Launder [34], Amano [4] and Yap [10] have demonstrated similar results when applying wall functions to abrupt pipe expansions. The WF2 and WF3 models show slightly better correlation to the St data relative to WF1. All three wall functions predict similar C_f profiles with the exception that downstream, beyond reattachment, WF3 predicts C_f closer to the data. As a result, the WF3 model predicts $St \approx 14\%$ higher at $x/H = 20$ relative to WF1. The results obtained using wall functions demonstrate that in complex flows, use of the low Reynolds number method does not necessarily lead to better results if the near-wall functions are based on u_τ or distance from the wall.

Figure 9(c) compares the St profiles predicted by the LS and LSY models. The LS model greatly over-

Table 12. Skin friction results for the backward facing step case

Model	Correlation coefficient r	% C_f @ minimum C_f	% C_f @ $x/H = 20$	% x/H reattachment length
WF1	0.96	5.1	−31.4	−10.5
WF2	0.97	−2.4	34.5	−9.9
WF3	0.97	−9.8	15.5	−15.6
CH	0.84	190.6	10.4	−10.2
LB	0.93	76.3	−0.3	−16.5
LS	0.79	135.1	−29.7	−16.8
LSY	0.95	66.8	−31.6	−6.3
MK	0.92	163.7	−16.2	9.9
WCP	0.96	35.4	−47.7	6.0
WX	0.99	8.6	−42.9	11.3

predicts the maximum St in the vicinity of reattachment (about 4.7 times too high). This result is consistent with the data reported by Chieng and Launder [3] who obtained heat transfer predictions in the vicinity of reattachment five times too high for an abrupt pipe expansion test case. The correction to the Chieng and Launder work by Johnson and Launder [34] was considered, but not included here. The addition to the Yap correction term to the LS model significantly improves the predicted St and C_f profiles. Even with this correction the LSY model poorly predicts C_f in the recirculation zone and does not calculate St as well as the models of either WX, WCP or the wall functions.

Figure 9(d) shows that both CH and MK models fail to predict the St distribution in the vicinity of reattachment. These models also substantially overestimate C_f, both in the recirculating flow region and directly after reattachment, Fig. 10. The models of CH and MK assume that the near-wall turbulence can be specified in terms of u_τ and therefore does not show the correct behavior in regions where the turbulence is not controlled by u_τ (the poor behavior of the damping functions used in the models of CH and MK is reflected in their numerical performance: both models took over double the number of iterations to converge relative to the WX model).

The backward facing step test case demonstrates, even more emphatically than the impinging slot jet test case, how poorly the models of CH, LB, LS and MK predict convection heat transfer when coupled with a complex turbulent flow. The WCP model predicts reasonable results, but underpredicts the heat transfer near reattachment. Only the WX model demonstrates strong performance on all three test cases.

6.4. *Programming and numerical considerations*

From the perspective of the programmer the WX model has several advantages. It does not include additional terms $\tilde{D}$ and $\tilde{E}$, thereby reducing the amount of coding required. The WX model determines its low Reynolds number effects through the turbulence Reynolds number R_t. All other low Reynolds number models, with the exception of LS, require calculation of the turbulence Reynolds number R_y or the dimensionless distance from the wall y^+. The models of CH and MK, which are based on y^+, require that at each iteration the wall shear stress τ_w be determined along these surfaces. As a result, the programming required to handle cases that are three-dimensional, involve complex geometry or blockages, becomes very tedious for models other than WX and LS.

The WX model produced a converged solution about 24% faster than the low Reynolds number k–ε models. This can partly be attributed to the ω-equation boundary condition (i.e. ω is fixed at the wall) and partly due to better behavior of the damping functions used to provide the low Reynolds number effects. This becomes especially important in the region very close to the wall (i.e. $y^+ < 1$). The main strength of WX in this respect is that the damping functions are all bounded between 'reasonable' values (i.e. $0.56 \leqslant \alpha \leqslant 2.2$, $0.025 \leqslant \alpha^* \leqslant 1$, $0.025 \leqslant \beta^* \leqslant 0.09$). In contrast, the damping function f_μ used in the models of LB and MK is not bounded. During the solution process, should R_t become very small, f_μ can become greater than unity providing unrealistic values of ν_t. The ε-equation boundary condition used in conjunction with LB and MK is a zero gradient boundary condition. The value of ε_w is therefore determined during the solution process and does not possess the stabilizing effect of a fixed wall boundary condition. In addition, the LB model's f_1 term is not bounded, should f_μ become very small, f_1 becomes large resulting in a large positive source term for the ε-equation.

The models of CH, LS and LSY all have bounded damping functions and the $\tilde{\varepsilon}$-equation has a fixed boundary condition at the wall. However to recover the correct values of k and ε at the wall the models of CH, LS and LSY employ the $\tilde{D}$ and $\tilde{E}$ terms. These models, therefore, are sensitive to the values calculated by the $\tilde{D}$ and $\tilde{E}$ terms, which increases the computational time required for convergence relative to the WX model. Further discussion of these items can be found in Heyerichs [35].

7. CONCLUSION

This paper has evaluated a number of variants to the k–ε and k–ω two-equation turbulence models and their ability to predict turbulent convection heat transfer in channel flow, impinging slot jet flow and flow downstream of a backward facing step. The general conclusions drawn are:

(1) The Wilcox model predicts turbulent convection heat transfer significantly better than the other models considered, calculating Nu within 2% for the channel flow test case and showing the highest correlation ($r \geqslant 95\%$) to the heat transfer for the impinging slot jet and backward facing step test cases.

(2) The Wilcox model is the easiest to implement since it does not require the calculation of the wall shear stress, distance from the wall or the additional terms $\tilde{D}$ and $\tilde{E}$. This simplifies the programming required to handle cases that are three dimensional, involve complex geometry or blockages.

(3) The Wilcox model demonstrates better convergence behavior, producing on average, converged solutions 24% faster relative to the other low Reynolds number models considered. The higher rate of convergence can be attributed to the bounded near-wall damping functions and the Dirichlet wall boundary condition applied to the ω-equation.

7.1. *Channel flow test case*

(1) All models predict reasonable results for the channel flow test case. Wall functions calculate C_f

within $\approx 2\%$ and show strong agreement with the log-law and temperature data of Kader [27]. This result can be anticipated since they are derived based on the log-law and temperature log-law, Jaytilleke [28]. All low Reynolds number models except LB and LSY predict C_f within 5% and $\approx 7\%$, respectively.

(2) When using the low Reynolds number approach, there is a strong correlation between a models ability to predict the log-law, C_f and Nu. The models of LB, LSY and MK that underpredict the log-law, overestimate C_f and Nu. On the other hand, the models of CH and LS that overestimate the log-law, underpredict C_f and Nu. The WCP model shows the best fit to the log-law and Nu is predicted to within $\approx 1\%$ of the Dittus–Boelter correlation.

(3) The temperature profile T^+ and Nu calculated by the low Reynolds number models are strongly influenced by the value of σ_t ($\approx -10\,\Delta Nu$ per $0.1\,\Delta\sigma_t$).

(4) None of the models predict both k^+ and ε^+ well in the near-wall region, indicating that further refinement of the near-wall damping functions is required.

(5) The standard k–ε model constants given by Launder and Spalding [2] overestimate ν_t in the central region of the channel. Changing the model constants as suggested by Yeung and Pollard [31] brings the ν_t prediction into close agreement with experimental data and decreases C_f and Nu by less than 1%. Similarly, the WX model overpredicts ν_t in the central region of the channel indicating that the constants suggested by Wilcox [16] also require adjustment.

7.2. *Impinging slot jet and backward facing step test cases*

(1) Only the WX model shows a high correlation ($r \geqslant 95\%$) to the experimental heat transfer data for the impinging slot jet and backward facing step case. The strong performance by the WX model indicates that near-wall functions based on the turbulence variables extrapolate better to conditions far from equilibrium than those that specify turbulence based on u_τ or distance from the wall. Wall functions and the models of CH, LB, LS, LSY and MK perform poorly and are not recommended for modelling complex flows.

(2) The WCP model fails to accurately predict heat transfer in the vicinity of stagnation and reattachment, implying that in complex flows, Wolfshtein's one-equation model does not adequately describe the near-wall region and transport equations for both velocity and length scale are required to calculate accurate results.

8. RECOMMENDATIONS

There is a need for more experimental turbulent convection heat transfer studies. A well-controlled, high Re, channel flow experiment is required to establish a single reliable data set that can be used to benchmark turbulence models and further refine near-wall damping functions and model constants. Such an experiment could also be used to obtain a better prescription of σ_t across the near-wall region, since use of a formula that varies σ_t with R_t, may lead to improved heat transfer predictions relative to those obtained based on the assumption that $\sigma_t = 0.9$. More reliable hydrodynamic and heat transfer data are required for turbulent impinging plane jets. The data should clearly specify if the secondary Nu peak is caused by relaminarization and boundary layer transition or impingement of vortex rings into the boundary layer.

Acknowledgement—This work was supported by the Natural Sciences and Engineering Research Council of Canada. The computations were performed on IBM R/S 6000 Model 590 and SGI 4D240GTX computers both of which belong to the Centre for Advanced Gas Combustion Technology, Queen's University. K.H. was granted a leave of absence from Dofasco Inc. to pursue graduate studies at Queen's University.

REFERENCES

1. V. C. Patel, W. Rodi and G. Scheuerer, Turbulence models for near-wall and low Reynolds number flows: a review, *AIAA J.* **23**(9), 1308–1319 (1985).
2. B. E. Launder and D. B. Spalding, The numerical computation of turbulent flows, *Comp. Meth. App. Mech. Engng* **3**, 269–289 (1974).
3. C. C. Chieng and B. E. Launder, On the calculation of turbulent heat transport downstream from an abrupt pipe expansion, *Numer. Heat Transfer* **3**, 189–207 (1980).
4. R. S. Amano, Development of a turbulence near-wall model and its application to separated and reattached flows, *Numer. Heat Transfer* **7**, 59–75 (1984).
5. H. C. Chen and V. C. Patel, Near-wall turbulence models for complex flows including separation, *AAIA J.* **26**(6), 641–648 (1988).
6. M. Wolfshtein, The velocity and temperature distribution in one-dimensional flow with turbulence augmentation and pressure gradient, *Int. J. Heat Mass Transfer* **12**, 301–318 (1969).
7. B. E. Launder and B. I. Sharma, Applications of the energy-dissipation model of turbulence to the calculation of flow near a spinning disc, *Lett. Heat Mass Transfer* **1**, 131–138 (1974).
8. C. K. G. Lam and K. A. Bremhorst, Modified form of the k–ε model for predicting wall turbulence, *J. Fluids Engng* **103**, 456–460 (1981).
9. K.-Y. Chien, Predictions of channel and boundary-layer flows with a low-Reynolds-number turbulence model, *AIAA J.* **20**, 33–38 (1982).
10. C. Yap, Turbulent heat and momentum transfer in recirculating and impinging flows, Ph.D. Thesis, Faculty of Technology, University of Manchester, U.K. (1987).
11. H. K. Myong and N. Kasagi, A new proposal for a k–ε turbulence model and its evaluation, *Trans. Jpn Soc. Mech. Engng* **54**(507), 3003 (1988).
12. A. N. Kolmogorov, Equations of turbulent motion of an incompressible fluid, *Izv. Akad. Nauk. SSR, Seria Fizicheska Vi*, (1/2) 56–58. (English translation: Imperial College, Mechanical Engineering Department. Report, ON/6, 1968) (1942).
13. D. B. Spalding, The prediction of two-dimensional, steady turbulent flows, Imperial College, Heat Transfer Section Report EF/TN/A/16 (1969).
14. Saiy, Turbulent mixing of gas streams, Ph.D. thesis, Imperial College, University of London (1974).
15. P. G. Saffman, A model for inhomogeneous turbulent flow. *Proc. R. Soc. Lond. Ser. A.* **317**, 417–433 (1970).

16. D. C. Wilcox, The remarkable ability of turbulence model equations to describe transition, DCW Industries Inc. La Cañada, CA (1992).
17. W. V. Patankar, *Numerical Heat Transfer and Fluid Flow*. Hemisphere, New York (1980).
18. A. Pollard and A. L.-W. Siu, The calculation of some laminar flows using various discretization schemes, *Comp. Meth. Appl. Mech. Engng* **35,** 293–313 (1982).
19. D. B. Spalding, A novel finite-difference formulation for differential expressions involving both first and second derivatives, *Int. J. Numer. Meth. Engng* **4,** 551 (1972).
20. J. P. Van Doormaal, and G. D. Raithby, Enhancements of the SIMPLE method for predicting incompressible fluid flows, *Numer. Heat Transfer* **7,** 147–163 (1984).
21. F. F. Cadek, A fundamental investigation of jet impingement heat transfer, Ph.D. Thesis, University of Cincinnati, U.S.A. (1968).
22. D. Das, Convective heat transfer under a turbulent impinging slot jet at large temperature differences, M.Eng. Thesis, McGill University, Montreal (1982).
23. R. Gardon and J. C. Akfirat, Heat transfer characteristics of impinging two-dimensional air jets, *Trans. ASME, J. Heat Transfer*, **88,** 101–108 (1966).
24. A. R. P. Van Heiningen, Heat transfer under an impinging slot jet, Ph.D. Thesis, McGill University, Montreal, Canada (1982).
25. J. C. Vogel and J. K. Eaton, Heat transfer and fluid mechanics measurements in the turbulent reattaching flow behind a backward-facing step, Report MD-44, Thermosciences Division, Department of Mechanical Engineering, Stanford University, Stanford, California, U.S.A. (1984).
26. M. N. Özişik, *Heat Transfer—a Basic Approach*. McGraw-Hill, New York (1985).
27. B. A. Kader, Temperature and concentration profiles in fully turbulent boundary layers, *Int. J. Heat Mass Transfer* **24**(9), 1541–1544 (1981).
28. C. L. Jayatilleke, The influence of Prandtl number and surface roughness on the resistance of the laminar sublayer to momentum and heat transfer, *Prog. Heat Mass Transfer* **1,** 193–329 (1969).
29. D. B. Spalding, Heat transfer from turbulent separated flows, *J. Fluid Mech.* **27,** 97–109 (1967).
30. N. Kasagi, Y. Tomita and A. Kuroda, Direct numerical simulation of passive scalar field in a turbulent channel flow, *ASME J. Heat Transfer* **114,** 598–606 (1992).
31. P. K. Yeung and A. Pollard, Empirical constants in the k–ε model for turbulent channel flow, Report TFG/90/1, Queens University (1990).
32. F. Hussain and W. C. Reynolds, Measurements in fully developed turbulent channel flow, *Trans. ASME, J. Fluids Engng* **97,** 568–580 (1975).
33. E. W. Adams, J. P. Johnston and J. K. Eaton, Experiments on the structure of turbulent reattaching flow, Report MD-43, Thermosciences Division, Department of Mechanical Engineering, Stanford University, Stanford CA, U.S.A. (1984).
34. R. W. Johnson and B. E. Launder, Discussion on the calculation of turbulent heat transport downstream from an abrupt pipe expansion, *Numer. Heat Transfer* **5,** 493–496 (1982).
35. K. Heyerichs, Modelling of convection heat transfer in complex turbulent flows, M.Sc. Thesis, Queens University Kingston, Ontario (1995).